Materials Chemistry and Physics 257 (2021) 123741

Contents lists available at ScienceDirect

Materials Chemistry and Physics

journal homepage: www.elsevier.com/locate/matchemphys

A novel synthesis route to obtain magnetic nanocrystalline cobalt ferrite with photo-Fenton activity

Bruna G. de Souza [a,b], Gustavo Figueira [c], Maria H. Carvalho [d], Victor Alcaraz-Gonzalez [e], Karla E. Saldaña-Flores [e], Mário Godinho Jr. [f], Adilson J.A. de Oliveira [d], Ruth H.G. A. Kiminami [c], Luís A.M. Ruotolo [a,*], Ernesto A. Urquieta-González [a,b,**]

[a] Department of Chemical Engineering, Federal University of São Carlos, C. Postal 676, CEP 13565-905, São Carlos, SP, Brazil
[b] Research Center on Advanced Materials and Energy, Federal University of São Carlos, C. Postal 676, CEP 13565-905, São Carlos, SP, Brazil
[c] Graduate Program in Materials Science and Engineering, Federal University of São Carlos, C. Postal 676, CEP 13565-905, São Carlos, SP, Brazil
[d] Department of Physics, Federal University of São Carlos, C. Postal 676, CEP 13565-905, São Carlos, SP, Brazil
[e] University of Guadalajara - CUCEI, Blvd. Marcelino G. Barragán 1421, 44430, Guadalajara, Mexico
[f] Institute of Chemistry, Federal University of Goiás, Av. Dr. Lamartine P. Avelar 1120, 75704-020, Catalão, GO, Brazil

HIGHLIGHTS

- Novel unconventional coprecipitation procedure to obtain cobalt ferrites.
- Room temperature and surfactant-free synthesis.
- MW-assisted hydrothermal treatment with octahedral Co^{2+} migration to tetrahedral sites.
- Superior incorporation of the highly active Fe^{3+} at the ferrite octahedral sites.
- Magnetic and photo-Fenton active cobalt ferrites photocatalysts.

GRAPHICAL ABSTRACT

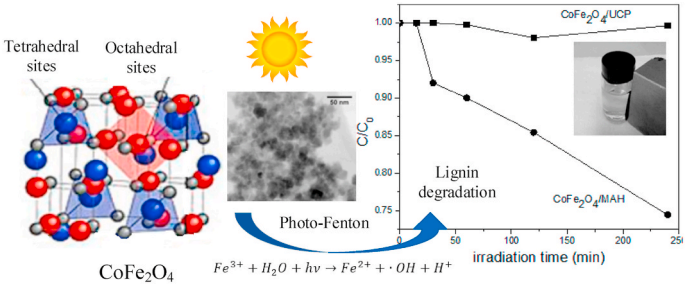

ARTICLE INFO

Keywords:
$CoFe_2O_4$
Unconventional coprecipitation
Microwave-assisted hydrothermal treatment
Photo-Fenton
Lignin degradation

ABSTRACT

A novel unconventional coprecipitation procedure (UCP) followed by a simple and fast microwave-assisted hydrothermal (MAH) treatment was used to synthesize a new nanocrystalline magnetic cobalt ferrite ($CoFe_2O_4$/MAH) with photo-Fenton activity. The Co-ferrite nanoparticles were obtained at room temperature in the absence of surfactants and their photo-Fenton activity was evaluated through lignin degradation. It was found that microwave hydrothermal treatment is mandatory to obtain magnetic and photoactive Co-ferrite. According to XRD Rietveld refinements and FTIR, the photoactivity was mainly attributed to the Co^{2+} cation migration from octahedral to tetrahedral sites in the ferrite structure during the MAH treatment, leading, consequently, to a higher Fe^{3+} incorporation at octahedral sites, which strongly participate in the photo-Fenton degradation mechanism. The magnetic property of the $CoFe_2O_4$/MAH ferrite nanoparticles was confirmed by magnetometry and provided an easy catalyst separation.

* Corresponding author.
** Corresponding author. Department of Chemical Engineering, Federal University of São Carlos, C. Postal 676, CEP 13565, São Carlos, SP, Brazil.
E-mail addresses: pluis@ufscar.br (L.A.M. Ruotolo), urquieta@ufscar.br (E.A. Urquieta-González).

https://doi.org/10.1016/j.matchemphys.2020.123741
Received 19 May 2020; Received in revised form 11 July 2020; Accepted 19 August 2020
Available online 11 September 2020

1. Introduction

Cobalt ferrites ($CoFe_2O_4$) emerged as promising heterogeneous catalysts for photo-Fenton reactions due to their chemical and physical stability, and magnetic properties, which could facilitate their separation from the reaction system by applying an external magnetic field [1]. Considering that the $CoFe_2O_4$ magnetic properties are strongly influenced by the particle size, the search for new synthesis procedures to obtain ferrite nanoparticles has been intensified in the last years [2,3].

Cobalt ferrites are usually synthesized by conventional coprecipitation adjusting the pH of a solution containing different metal cations, thus leading to a selective coprecipitation [4,5]. According to this procedure, a solid solution is seldom formed and requires further thermal treatment. In this work, we propose a novel synthesis route involving an unconventional coprecipitation (UCP) [6] technique in which the cations are added into a very alkaline medium, promoting instantaneous cations coprecipitation as incipient nuclei of the ferrite phase, with ferrite crystallization being consolidated after aging at room temperature. In order to obtain a magnetic photocatalyst, the ferrite was submitted to a microwave-assisted hydrothermal (MAH) treatment. Besides enhancing the nucleation rate, the microwave (MW) radiation leads to more uniform ferrite nucleation with faster crystallization kinetics. Furthermore, the MW radiation also promotes faster and uniform heating of the reaction medium, thus decreasing the synthesis time and operational cost [4]. To the best of our knowledge, this is the first time that a synthesis route combining the proposed UCP and MAH procedures is applied to obtain cobalt ferrite nanoparticles with promising textural, structure, and magnetic properties to be applied as a photo-Fenton catalyst.

The photo-Fenton activity was tested for lignin degradation as proof of concept. Lignin was chosen as a model recalcitrant organic pollutant commonly found in many wastewaters. The photo-Fenton is characterized by the presence of H_2O_2 and Fe^{2+} in the reaction medium, which is illuminated using UV radiation to generate very oxidant species, mainly the hydroxyl radicals $^{\bullet}OH$, as shown in Eqs. (1) and (2).

$$Fe^{3+} + H_2O + h\nu \rightarrow Fe^{2+} + \cdot OH + H^+ \quad (1)$$

$$H_2O_2 + h\nu \rightarrow 2 \cdot OH \quad (2)$$

Homogeneous photo-Fenton, despite the high reaction rates, simplicity, and efficacy, has the inconvenience that iron cannot be easily recovered or removed from the catalytic system after the reaction. In order to overcome this issue, heterogeneous Fe catalysts have been developed but imposing a new challenge regarding the separation and recovery of the nanoparticles from the reaction system [1]. This issue stimulated the research for ferrite photocatalysts with magnetic properties.

In this context, we investigated and proposed a novel synthesis route to obtain magnetic nanocrystalline cobalt ferrite by applying at room temperature the previously mentioned surfactant-free UCP, followed by aging and MAH procedures. The as-synthesized ferrites were analyzed by XRD with Rietveld refinement, FTIR, SEM/EDS, TEM, and N_2 adsorption-desorption measurements. The magnetic properties were confirmed by magnetometry. The UCP cobalt ferrite $CoFe_2O_4$/UCP was firstly evaluated as catalyst for the photo-Fenton degradation of lignin. In order to verify whether the catalytic performance could be improved by the MW hydrothermal treatment, lignin photo-Fenton degradation was further investigated using the $CoFe_2O_4$/MAH ferrite.

2. Experimental

2.1. Materials

Ferric nitrate monohydrate (98%, Sigma-Aldrich™), cobalt nitrate hexahydrate (98%, Sigma-Aldrich™), sodium hydroxide (99%, Ensure™) and sulfuric acid (95–97%, Ensure™) were used to synthesize the cobalt ferrites. Alkaline lignin (Sigma-Aldrich™) and hydrogen peroxide (29%, Synth™) were used in the photo-Fenton degradation tests. All solutions were prepared using deionized water.

Table 1
Space group and atomic fractional coordinates (x, y, z) used in the Rietveld refinement applied to the cobalt ferrites XRD data [8].

Ferrite	Space group	ITC[a] number	x = y = z				
			16 d octahedral sites		8a tetrahedral sites		32e
$CoFe_2O_4$	$Fd\bar{3}m$	No. 227	Fe^{3+} 0.5000	Co^{2+}	Fe^{3+} 0.1250	Co^{2+}	O 0.2566

[a] International Tables for Crystallography.

2.2. Synthesis procedure

$CoFe_2O_4$/UCP was obtained at room temperature via the proposed UCP technique, in which Fe (III) and Co (II) nitrate solutions (62 mmol and 31 mmol, respectively) were mixed and added dropwise to 140 mL of 5.0 mol L^{-1} NaOH solution under vigorous stirring for 1 h (pH = 14). The resultant suspension containing the coprecipitate was then aged at room temperature for 48 h, filtrated, rinsed with distilled water until pH = 7, and dried at 100 °C for 24 h. The $CoFe_2O_4$/MAH was obtained submitting part of the coprecipitate suspension to a hydrothermal treatment at 130 °C for 30 min in a microwave oven (1300 W, Brastemp®). After the MW treatment, the material was aged, separated, rinsed, and dried following the same procedure previously described for the $CoFe_2O_4$/UCP sample.

2.3. Characterization

The as-obtained cobalt ferrite samples were characterized by XRD using a Rigaku Miniflex 600 Diffractometer operated using a Ni-filtered Cu Kα radiation (λ = 0.1542 nm), in a 2θ angle ranging from 25 to 80°, with a scan rate of 0.02° s^{-1}. A Rietveld refinement based on the Williamson-Hall method [7] applied to the ferrite X-ray powder diffraction data was accomplished using the PDXL software (Rigaku Corporation). The fractional atomic coordinates used for both ferrites are listed in Table 1. The oxygen positions (x = y = z) were taken as free parameters for the fitting while all the other atomic fractional positions were fixed. Other parameters related to the ferrite lattice, occupancies, scale factors, and shape were also taken as free. The peak shapes were described by a pseudo-Voigt function. Overall, the following sequence was adopted for the application of the Rietveld refinement: (i) profile and background; (ii) lattice parameter and scale factor; (iii) crystallite size; (iv) oxygen position, and (v) cation occupancies.

The cobalt ferrite nanoparticles were examined by FE-SEM using a Supra 35-VP Carl Zeiss equipment and the chemical composition determined by an Energy Dispersive X-ray Spectroscopy (EDS) modulus coupled to a Philips XL-30 FEG microscope. TEM images were obtained on a TECNAI G2 F20 transmission electron microscope equipped with a field emission gun (FEG) and operating at 200 kV. FTIR spectra, in the region from 50 to 4000 cm^{-1} with a resolution of 4 cm^{-1} and by co-adding 32 scans, were obtained by Diffuse Reflectance Infrared Fourier Transform (DRIFT) spectroscopy on a Bruker (Vertex 70) spectrometer having a DLaTGS detector. N_2 adsorption-desorption measurements were performed at the boiling nitrogen temperature (−196 °C) in a Micromeritics (ASAP 2420) apparatus. Prior to the analysis, the samples were degassed at 300 °C for 3 h to remove water and physically adsorbed gases. The ferrites specific surface areas were calculated from the Brunauer-Emmett-Teller (BET) equation in the range $0.05 < p/p_0 < 0.30$. Magnetization measurements up to 70 kOe were performed at room temperature using a SQUID-VSM magnetometer (MPMS® 3-Quantum Design).

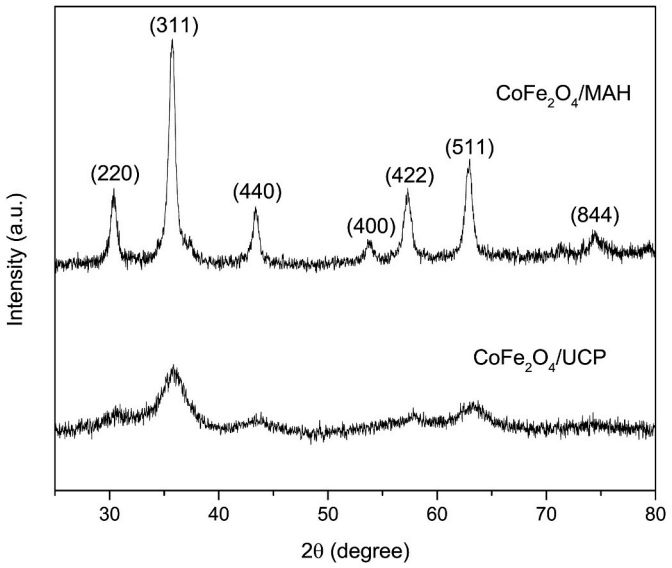

Fig. 1. XRD patterns of the cobalt ferrites synthesized by the UCP or UCP + MAH procedures.

2.4. Photo-fenton catalytic activity

The photo-Fenton activity was evaluated at 27 °C by suspending the ferrites (500 mg L^{-1}) into 0.04 L of a lignin solution (100 mg L^{-1}) with the pH adjusted to 3. The suspension was stirred in an orbital shaker equipped with four low-pressure mercury lamps (UVC TUV 15 W) positioned above the reaction vessels. The reaction started when a H_2O_2 solution (977 mg L^{-1}) was added. All the experiments were performed in duplicate. After the separation of the catalyst particles by centrifugation and membrane filtration, the remaining lignin in the liquid phase was analyzed by measuring the absorbance at 280 nm (Ultrospec 2100 *pro* spectrophotometer).

3. Results and discussion

According to the XRD patterns shown in Fig. 1, both ferrites present diffraction peaks corresponding to the atomic planes of a cubic spinel structure. The absence of peaks corresponding to secondary phases suggests that only pure ferrites were obtained. The crystalline structure of the ferrite is described by the $Fd\bar{3}m$ space group, thus the COD 1533163 was used in the Rietveld refinement [8].

Contrary to the high temperatures employed to treat the coprecipitate obtained by conventional ferrite syntheses [9], in this work the cobalt ferrites were obtained using the proposed UCP synthesis route, notably in absence of surfactants and at room temperature. After the MW hydrothermal treatment of the $CoFe_2O_4$/UCP ferrite, more intense and well-resolved diffraction peaks are observed for the $CoFe_2O_4$/MAH ferrite, thus indicating a crystallinity improvement. Indeed, the MW radiation enhances the nucleation rate, forming more uniform nuclei and resulting in a faster crystallization kinetics [10].

After the application of the Rietveld refinement, the structural features of the ferrites were determined and they are displayed in Table 2. The quality of the refinement is confirmed by the reliability factors R_{wp} and χ^2. As can be seen, the lattice parameter of the cubic spinel ferrite structure increased from 0.8321 to 0.8387 nm after the MAH treatment due to cations migration between tetrahedral and octahedral interstitial sites of the ferrite crystalline structure, as was also found by Abbas et al. [11]. According to Table 2, the Co^{2+} cations in the $CoFe_2O_4$/UCP ferrite occupy only their preferred octahedral sites [12], while Fe^{3+} occupies both, octahedral and tetrahedral sites. Interestingly, after the MW hydrothermal treatment, 30.3% of the tetrahedral sites in the structure of the $CoFe_2O_4$/MAH ferrite are occupied by Co^{2+} cations, thus evidencing the occurrence of cations migration between the ferrite interstitial sites, that resulted in a substantial increase of the Fe^{3+} cation content in the octahedral sites.

Regarding the crystalline structure of the ferrites, the FTIR spectra in Fig. 2 show the absorption bands below 1000 cm^{-1}. The vibrations at 500-600 cm^{-1} and 400-490 cm^{-1} are attributed to cations at tetrahedral (ν_1) and octahedral sites (ν_2), respectively [13]. These bands are more intense for the $CoFe_2O_4$/MAH ferrite, confirming the crystallinity improvement promoted by the MAH treatment, as previously pointed out during the discussion of the ferrites XRD diffractograms. Moreover, Fig. 2 also shows that the absorption bands in the $CoFe_2O_4$/MAH ferrite spectrum shift to lower wavenumbers, which is a consequence of the enlargement of the radius of the interstitial sites [14], that reduces the fundamental frequency of the chemical bonding. This behavior gives further evidence of the Co^{2+} and Fe^{3+} migration between tetrahedral and octahedral sites in the Co-ferrite structure during the MAH treatment, thus corroborating the Rietveld refinement results [15]. Hence, the structural formula of the $CoFe_2O_4$/MAH ferrite can be written as $(Co^{2+}_{y}Fe^{3+}_{1+y})$ $(Co^{2+}_{1-y}Fe^{3+}_{1-y})$ $(O^{2-})_4$, in which y is the degree of inversion or migration of Co^{2+} to tetrahedral sites, which implies in a

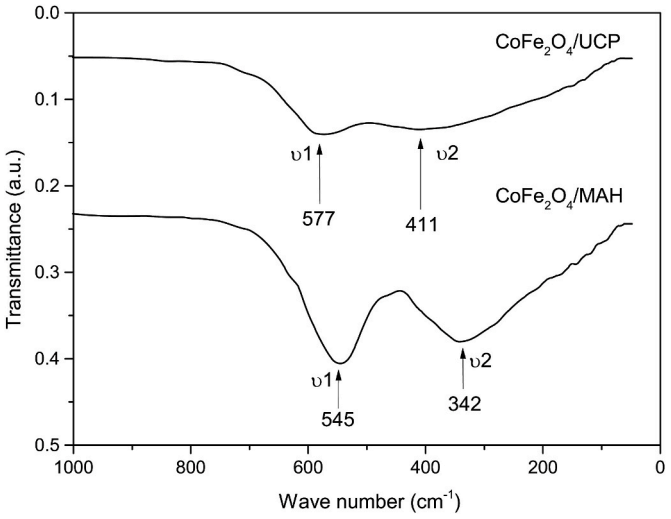

Fig. 2. FTIR spectra of the cobalt ferrites synthesized by the UCP or UCP + MAH procedures.

Table 2
Structural parameters and cation distribution based on the Rietveld refinement applied to the cobalt ferrites XRD data.

Sample	Crystallite size (nm)	Lattice parameter (nm)	Cation Occupancies[a]					Refinement quality index	
			16 d Octahedral sites		8a Tetrahedral sites		32e		
			Fe^{3+}	Co^{2+}	Fe^{3+}	Co^{2+}	O	χ^2	R_{wp} %
$CoFe_2O_4$/UCP	2.40	0.8321	0.130	0.870	1.000	0.000	1.000	2.64	3.72
$CoFe_2O_4$/MAH	12.0	0.8387	0.579	0.421	0.697	0.303	1.000	1.08	2.54

[a] The given values refer to the occupancy fraction.

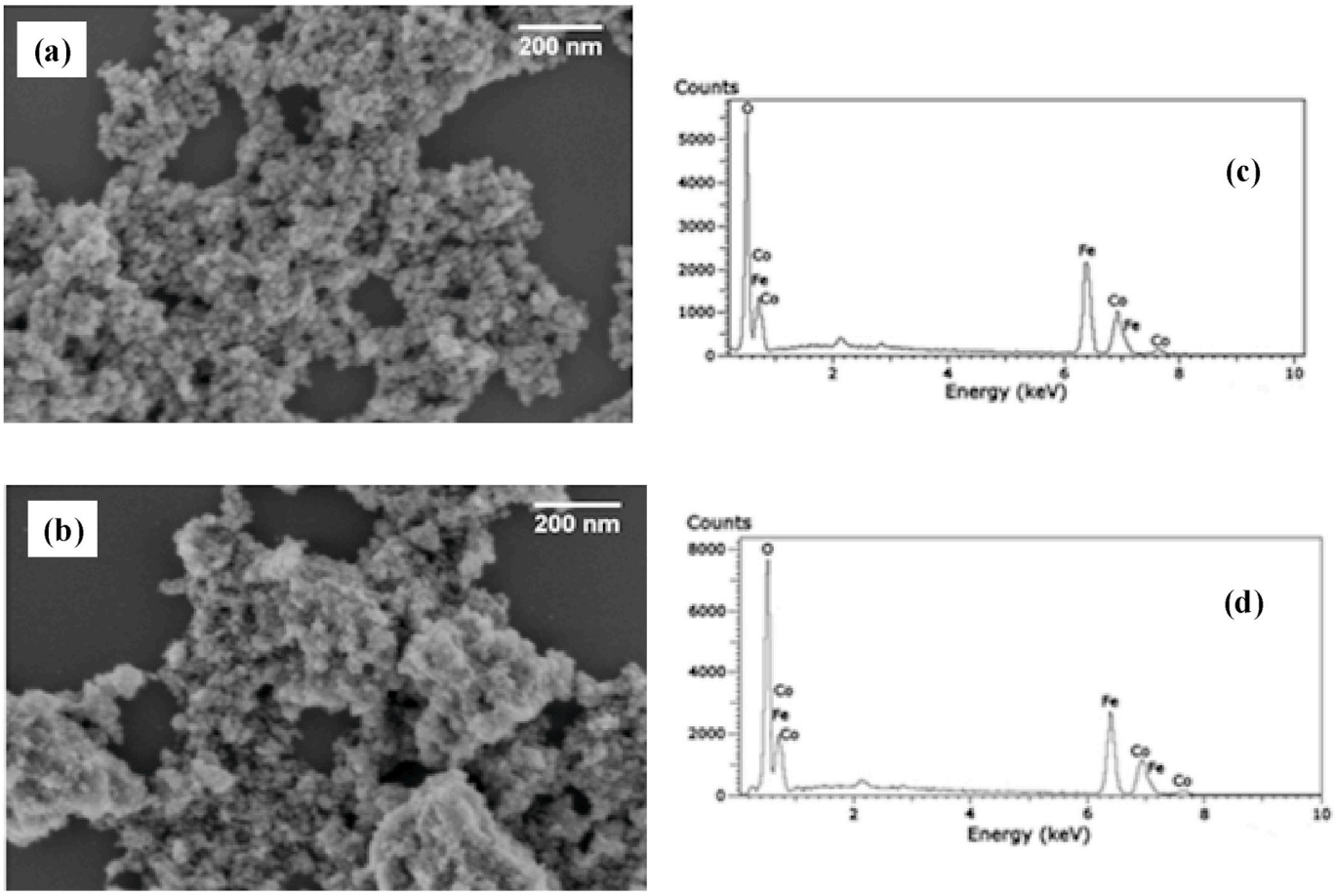

Fig. 3. FE-SEM images and EDS spectra of the synthesized cobalt ferrites: (a) and (b) $CoFe_2O_4$/MAH; (c) and (d) $CoFe_2O_4$/UCP.

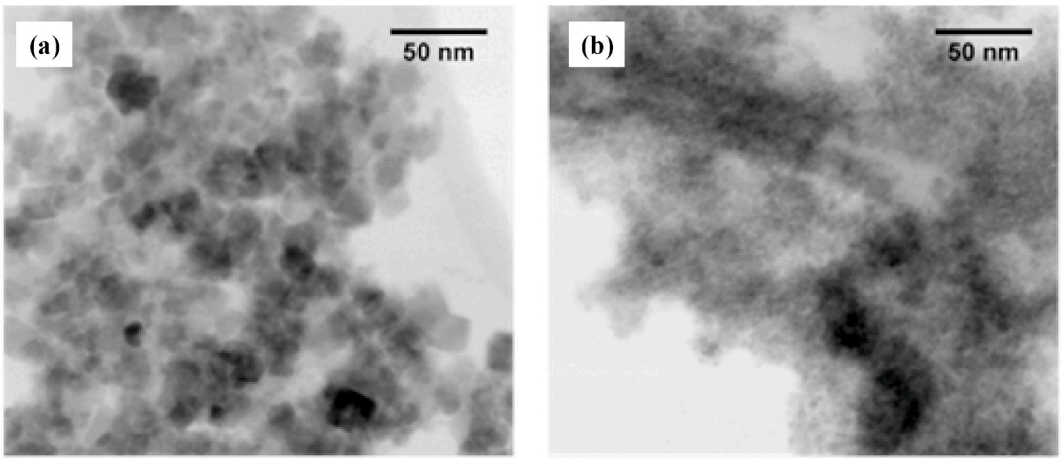

Fig. 4. TEM images of the synthesized cobalt ferrites: (a) $CoFe_2O_4$/MAH; (b) $CoFe_2O_4$/UCP.

smaller distortion of the crystalline structure. Considering that this phenomenon was also observed for a cobalt ferrite submitted to a conventional thermal treatment above of 300 °C [16], it was assumed that the MAH treatment promotes a similar effect, but at a lower temperature.

The SEM micrographs in Fig. 3a–c shows larger particle agglomerates for the $CoFe_2O_4$/MAH ferrite, and the EDS spectra (Fig. 3b–d) only the presence of cobalt, iron, and oxygen, evidencing the Co-ferrites purity. Furthermore, according to the TEM micrographs displayed in Fig. 4, the agglomerates are formed by roughly spherical particles with similar morphology, but with different sizes. The diameter of the $CoFe_2O_4$/MAH particles (10–15 nm) is remarkably larger than the $CoFe_2O_4$/UCP particles (<5 nm). In both cases, the particle sizes are in good agreement with those calculated from the Rietveld refinement, which are displayed in Table 1. The $CoFe_2O_4$/MAH particle size is also smaller than that of ferrites obtained by conventional hydrothermal [16] or thermal treatments [17], in which the particles grow with inhomogeneous heating and in a medium having insufficient crystallite seeds [18]. Using the MAH treatment after coprecipitation and subsequent aging, the crystallization improves due to the volumetric and

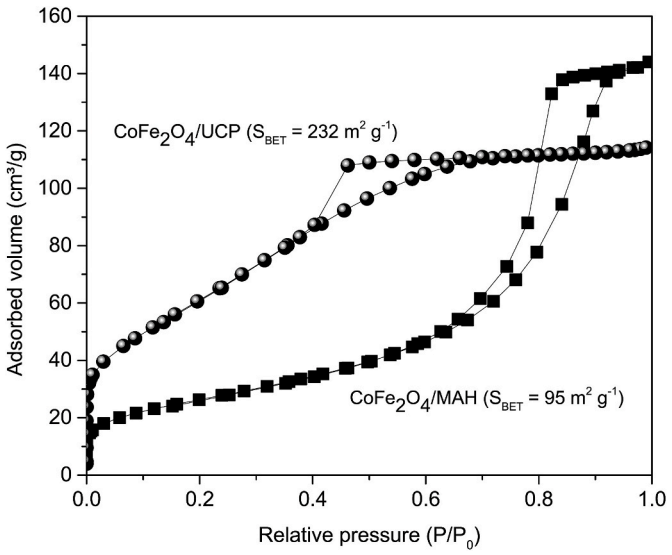

Fig. 5. N_2 adsorption/desorption isotherms of the studied cobalt ferrites.

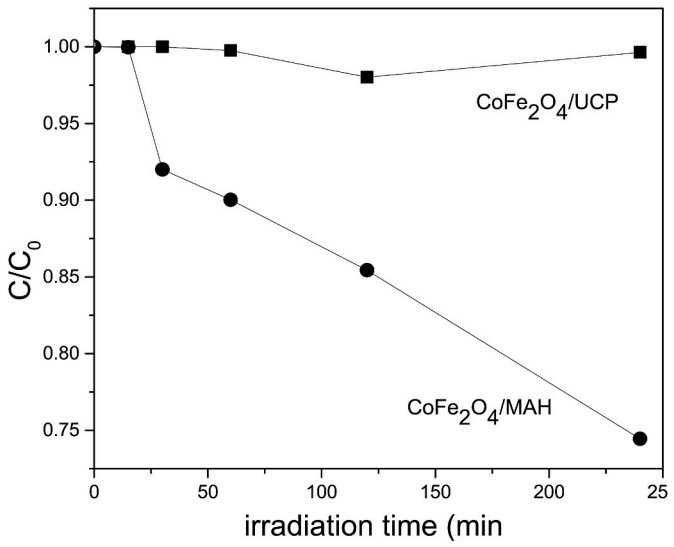

Fig. 7. Lignin degradation as a function of the irradiation time for the studied cobalt ferrites.

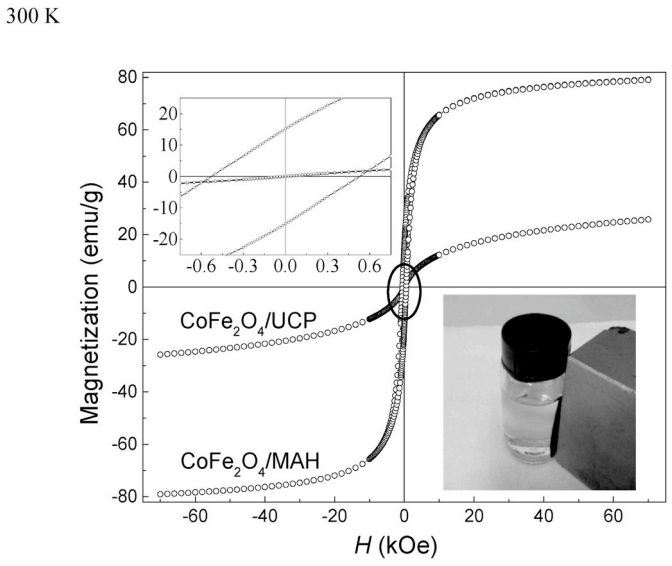

Fig. 6. Magnetization as a function of the applied magnetic field performed at room temperature for the $CoFe_2O_4$/UCP and $CoFe_2O_4$/MAH ferrites. Inset plot: Magnification in the low magnetic field region. Inset image: Magnetic recovery of the $CoFe_2O_4$/MAH ferrite from the photo-Fenton reaction system.

homogeneous heating promoted by the MW radiation, resulting in a narrower particle size distribution and more uniform morphology.

The textural properties of the cobalt ferrites were assessed from the N_2 adsorption/desorption isotherms shown in Fig. 5. Both ferrites show type IV isotherms indicating that after the UCP or UCP + MAH procedures, a mesoporous material was obtained. The H1 and H2 hysteresis loops indicate, respectively, the presence of regular cylindrical pores or narrow pores with wide sections for the $CoFe_2O_4$/MAH and $CoFe_2O_4$/UCP ferrites [8]. The reduction of the specific surface area from 232 to 95 $m^2 g^{-1}$ after the MAH treatment is mainly explained by the increase of the crystallite size from 2.40 to 12.0 nm due to the growth of the well-formed crystallites during the MAH treatment, as a consequence of the dissolution of the smaller ones [19].

The magnetic property is important in order to facilitate the catalyst recovery after the reaction process. Fig. 6 shows the magnetization of the studied ferrites as a function of the magnetic field. The coercive field (H_C) and remnant magnetization (M_r) can be seen in the inset plot in Fig. 6. The hysteresis curve for the $CoFe_2O_4$/MAH ferrite exhibits a H_C = 529 Oe and a M_r = 15.1 emu/g, which are typical values of ferrimagnetic cobalt ferrites [20,21]. Moreover, the nanoparticles are easily separated from the liquid phase using a magnetic field, as shown in the illustrative inset image in Fig. 6. On the other hand, H_C and M_r were not observed for the $CoFe_2O_4$/UCP ferrite, indicating that this material is in its superparamagnetic state, i.e., the magnetization of the nanoparticles floats by thermal excitation, thus presenting properties analogous to a paramagnetic material, but in this case, exhibiting a much larger effective magnetic moment.

Finally, the ferrites were tested regarding their photo-Fenton activity. According to Fig. 7 the $CoFe_2O_4$/UCP ferrite practically did not show photocatalytic activity, while ~25% of the lignin was degraded over the $CoFe_2O_4$/MAH ferrite, confirming its potential activity for the photo-Fenton reaction [22].

It is also important to notice that the photocatalytic behavior of $CoFe_2O_4$/MAH cannot be attributed to a surface area effect since the nanoparticles of this ferrite are larger than the $CoFe_2O_4$/UCP and, consequently, the illuminated surface is lower. These trends revealed the paramount importance of the MAH treatment to obtain an active heterogeneous catalyst for the photo-Fenton reaction, thus confirming that the redox properties of the $CoFe_2O_4$/MAH ferrite were a consequence of Fe^{3+} cations occupying the octahedral sites of the ferrite spinel structure. Indeed, the superior catalytic activity of $CoFe_2O_4$/MAH ferrite was due to the higher Fe^{3+} content at the octahedral sites of its crystalline structure, as was evidenced by Rietveld refinements (Table 2) and FTIR analyses (Fig. 2). The increase of the Fe^{3+} occupancy in the octahedral sites in the ferrite structure was a consequence of the migration of Co^{2+} from their preferred octahedral occupancy to tetrahedral sites during the MAH treatment, with the generated octahedral vacancies being occupied by the Fe^{3+} cations.

4. Conclusion

A novel synthesis route was proposed and successfully employed to prepare magnetically recoverable cobalt ferrite nanoparticles with photo-Fenton catalytic activity. Employing an unconventional Fe^{3+} and Co^{2+} coprecipitation method at pH = 14, combined with aging at room temperature and microwave-assisted hydrothermal treatment, the active ferrite $CoFe_2O_4$/MAH was obtained. The XRD patterns showed that the proposed synthesis allowed the formation of cobalt ferrite at room temperature and in the absence of surfactants. The ferrite

crystallinity was improved after the MAH treatment as well as the photo-Fenton catalytic activity for lignin degradation. The superior performance of the $CoFe_2O_4$/MAH ferrite was ascribed to the higher Fe^{3+} incorporation at the octahedral sites of the ferrite structure, as was supported by Rietveld refinements and corroborated by FTIR analyses.

CRediT authorship contribution statement

Bruna G. de Souza: Methodology, Formal analysis, Synthesis, characterization, ferrites catalytic evaluation, results analysis, Editing, and writing. **Gustavo Figueira:** Formal analysis, Characterization, and results analysis. **Maria H. Carvalho:** Characterization, and results analysis. **Victor Alcaraz-Gonzalez:** Formal analysis, Ferrites catalytic evaluation, results analysis and, writing. **Karla E. Saldaña-Flores:** catalytic evaluation, and results analysis. **Mário Godinho:** Jr, Methodology, Formal analysis, synthesis, and results analysis. **Adilson J.A. de Oliveira:** Characterization, and results analysis. **Ruth H.G.A. Kiminami:** Formal analysis, Synthesis, characterization, results analysis and, writing. **Luís A.M. Ruotolo:** Characterization, Conceptualization, Formal analysis, Writing - original draft, editing, and, Visualization. **Ernesto A. Urquieta-González:** Formal analysis, Methodology, results analysis, writing, review, editing, Supervision, Project administration, and, Funding acquisition.

Declaration of competing interest

The authors declare that they have no known competing financial interests or personal relationships that could have appeared to influence the work reported in this paper.

Acknowledgment

The authors thank FAPESP, Brazil, for the financial support (Grants 2017/24995–2, 2017/13769–1, 2013/07296–2, and 2009/54082–2). B.G.S. thanks the support given by the SWINDON-EXCEED DAAD Project (Germany) for the mobility training at the Federal University of Santa Maria (Brazil) and Guadalajara University (Mexico) and to CAPES, Brazil, for the Ph.D. fellowship (finance code 001). The authors also thank William N. Castelblanco for the Rietveld refinements.

References

[1] V.K. Sharma, R. Doong, H. Ki, R.S. Varma, D.D. Dionysiou, Ferrites and Ferrates: Chemistry and Applications in Sustainable Energy and Environmental Remediation, in: ACS Symposium Series, American Chemical Society, Washington, 2016.

[2] A. Scano, V. Cabras, M. Pilloni, G. Ennas, Microemulsions: the renaissance of ferrite nanoparticle synthesis, J. Nanosci. Nanotechnol. 19 (2019) 4824–4838, https://doi.org/10.1166/jnn.2019.16876.

[3] V. Mameli, M.S. Angotzi, C. Cara, C. Cannas, Liquid phase synthesis of nanostructured spinel ferrites - a review, J. Nanosci. Nanotechnol. 19 (2019) 4857–4887, https://doi.org/10.1166/jnn.2019.16808.

[4] E. Casbeer, V.K. Sharma, X.Z. Li, Synthesis and photocatalytic activity of ferrites under visible light: a review, Separ. Purif. Technol. 87 (2012) 1–14, https://doi.org/10.1016/j.seppur.2011.11.034.

[5] L. Zhang, X. Zhou, X. Guo, X. Song, X. Liu, Investigation on the degradation of acid fuchsin induced oxidation by $MgFe_2O_4$ under microwave irradiation, J. Mol. Catal. 335 (2011) 31–37, https://doi.org/10.1016/j.molcata.2010.11.007.

[6] S. Zhang, H. Niu, Y. Cai, X. Zhao, Y. Shi, Arsenite and arsenate adsorption on coprecipitated bimetal oxide magnetic nanomaterials: $MnFe_2O_4$ and $CoFe_2O_4$, Chem. Eng. J. 158 (2010) 599–607, https://doi.org/10.1016/j.cej.2010.02.013.

[7] L. Kumar, P. Kumar, M. Kar, Cation distribution by Rietveld technique and magnetocrystalline anisotropy of Zn substituted nanocrystalline cobalt ferrite, J. Alloys Compd. 551 (2013) 72–81, https://doi.org/10.1016/j.jallcom.2012.10.009.

[8] T. Ferreira, J. Waerenborgh, M. Mendonça, M. Nunes, F. Costa, Structural and morphological characterization of $FeCo_2O_4$ and $CoFe_2O_4$ spinels prepared by a coprecipitation method, Solid State Sci. 5 (2003) 383–392, https://doi.org/10.1016/S1293-2558(03)00011-6.

[9] N. Dahal, S. García, J. Zhou, S.M. Humphrey, Beneficial effects of microwave-assisted heating versus conventional heating in noble metal nanoparticle synthesis, ACS Nano 6 (2012) 9433–9446, https://doi.org/10.1021/nn3038918.

[10] E. Manova, T. Tsoncheva, D. Paneva, M. Popova, N. Velinov, B. Kunev, Nanosized copper ferrite materials: mechanochemical synthesis and characterization, J. Solid State Chem. 184 (2011) 1153–1158, https://doi.org/10.1016/j.jssc.2011.03.035.

[11] Y.M. Abbas, S.A. Mansour, M.H. Ibrahim, S.E. Ali, Microstructure characterization and cation distribution of nanocrystalline cobalt ferrite, J. Magn. Magn Mater. 323 (2011) 2748–2756, https://doi.org/10.1016/j.jmmm.2011.05.038.

[12] I.C. Nlebedim, N. Ranvah, P.I. Williams, Y. Melikhov, J.E. Snyder, A.J. Moses, Effect of heat treatment on the magnetic and magnetoelastic properties of cobalt ferrite, J. Magn. Magn Mater. 322 (2010) 1929–1933, https://doi.org/10.1016/j.jmmm.2010.01.009.

[13] S. Rana, J. Philip, B. Raj, Micelle based synthesis of cobalt ferrite nanoparticles and its characterization using Fourier Transform Infrared Transmission Spectrometry and Thermogravimetry, Mater. Chem. Phys. 124 (2010) 264–269, https://doi.org/10.1016/j.matchemphys.2010.06.029.

[14] L. Kumar, P. Kumar, A. Narayan, M. Kar, Rietveld analysis of XRD patterns of different sizes of nanocrystalline cobalt ferrite, Int. Nano Lett. 3 (2013) 1–12.

[15] D.L. Dorset, X-Ray Diffraction: A Practical Approach, Cambrigde University Press, Cambridge, 1998.

[16] L.Y. Meng, B. Wang, M.G. Ma, K.L. Lin, The progress of microwave-assisted hydrothermal method in the synthesis of functional nanomaterials, Mater Today Chem 1–2 (2016) 63–83, https://doi.org/10.1016/j.mtchem.2016.11.003.

[17] C. Orbeci, I. Untea, G. Nechifor, A.E. Segneanu, M.E. Craciun, Effect of a modified photo-Fenton procedure on the oxidative degradation of antibiotics in aqueous solutions, Separ. Purif. Technol. 122 (2014) 290–296, https://doi.org/10.1016/j.seppur.2013.11.020.

[18] P.S. Rahim, A.R. Abdul, W.M.A. Wan Daud, Review on the main advances in photo-Fenton oxidation system for recalcitrant wastewaters, J. Ind. Eng. Chem. 21 (2015) 53–69, https://doi.org/10.1016/j.jiec.2014.05.005.

[19] C. Rath, S. Anand, R.P. Das, K.K. Sahu, S.D. Kulkarni, S.K. Date, Dependence on cation distribution of particle size, lattice parameter, and magnetic properties in nanosize Mn–Zn ferrite, J. Appl. Phys. 91 (2002) 2211–2215, https://doi.org/10.1063/1.1432474.

[20] F.G. Silva, J. Depeyrot, A.F.C. Campos, R. Aquino, D. Fiorani, D. Peddis, Structural and magnetic properties of spinel ferrite nanoparticles, J. Nanosci. Nanotechnol. 19 (2019) 4888–4902, https://doi.org/10.1166/jnn.2019.16877.

[21] B.J. Rani, M. Ravina, B. Saravanakumar, G. Ravi, V. Ganesh, S. Ravichandran, Ferrimagnetism in cobalt ferrite ($CoFe_2O_4$) nanoparticles, Nano-Struct Nano-Obj 14 (2018) 84–91, https://doi.org/10.1016/j.nanoso.2018.01.012.

[22] A. Zhang, L. Zhu, Z. Nan, Ni-doped Fe_3O_4 nanoparticles coupled with SnS_2 nanosheets as 0D/2D heterogeneous catalyst for photo-Fenton reaction, Mater. Chem. Phys. 224 (2019) 156, https://doi.org/10.1016/j.matchemphys.2018.12.008.